



An Applied Analytical Method for the Forward Extrusion of Metals

Amin Seyyed Nosrati, Karen Abrinia, and Ali Parvizi

(Submitted October 18, 2019; Accepted: 3 February 2020; published online February 18, 2020)

An applied analytical formulation was developed to deal with the forward extrusion of non-symmetric sections based on the upper bound method. This method of solution has been developed as an alternative to finite element method with the advantages of less time consumption and expense. The deforming region where the material flow occurs was formulated in a new and more realistic fashion by streamlines and stream surfaces. Streamlines and stream surfaces were defined parametrically for the material flow and the development of the kinematically admissible velocity field. The newly developed velocity field incorporated features such that the real physical aspects of the problem were followed more closely than before. The internal, shear and frictional power terms were obtained from the upper bound solution. Using the present method of analysis, the pattern of material flow and the relative extrusion pressure were computed. Results compared to previous works indicated substantial improvements. Experimental and numerical investigations were carried out, and the proposed theoretical model was verified. Close agreement was observed between the analytical results and those from the simulation and the experiment.

Keywords extrusion, finite element analysis, material flow, upper bound

1. Introduction

Considering different bulk forming processes, forward extrusion has been a favorite method, producing profiles with a variety of sections from a round billet in modern days. In extrusion industry, the analysis of the material flow behavior is not easily possible due to the complexity of the exit section and inhomogeneity of the deformation process. In addition, since die design and fabrication is generally carried out using the experience of the operators, it is not possible to find an optimal die profile to obtain minimum extrusion pressure and high quality products. Therefore, process engineers need to use a suitable tool for analyzing the process that is both faster and less time-consuming than the present trial and error methods. The various numerical and analytical methods have been applied to solve such problems. Some researchers have tried to perform numerical study into the extrusion process to predict the extrusion pressure (Ref 1–3), material flow behavior (Ref 4, 5), optimal die design (Ref 6–8) and defects (Ref 9, 10). The numerical methods which have been applied to analyze the metal extrusion processes were time-consuming and costly. In addition to numerical methods, the analytical methods based on upper bound approach (Ref 11) have been widely used by scholars to analyze the extrusion process. The majority of the analytical methods have been limited to predicting the extrusion load or to simple geometries and boundary conditions.

This is due to the complexity of the non-symmetric three-dimensional material flow in such problems. Therefore, it seemed to be necessary to provide a better analytical method of solution in order to overcome the present challenges in the extrusion industry. The analytical investigation of the extrusion process based on the upper bound method in previous works is reviewed in here.

Chitkara and Celik (Ref 12) employed the upper bound method to predict the extrusion pressure and optimum die design in forward extrusion process. They obtained kinematically admissible velocity fields for extrusion of non-symmetric T-shaped sections through streamlined dies. They investigated the effects of reduction of area, friction factor, die length and die positioning on the minimum extrusion load and die design. Ajiboye and Adeyemi (Ref 13) performed a theoretical study based on the upper bound method on the extrusion of round to shaped sections to investigate the effect of die land length on the extrusion pressure and flow pattern. They considered the frictional power at die land in the formulation for the analysis of the extrusion process. The authors concluded that the extrusion pressure increased with an increase in die land length. Abrinia and Davarzani (Ref 14) applied the upper bound analysis to find solutions for the extrusion of non-symmetric profiled sections using both flat faced and bilinear dies. They proposed the new method for discretizing the deforming region in order to formulate a kinematically admissible velocity field. The extrusion pressure and optimum die cavity was obtained using this method. Abrinia and Ghorbani (Ref 15) carried out an analytical and experimental investigation on the forward extrusion of non-symmetric profiled sections. The concept of their proposed formulation was that all points on the cross section of the initial billet transfer to similar points on the final cross section of the extruded product. They suggested the new method for dividing the deforming region into subsections in order to formulate a kinematically admissible velocity field and predict the material flow realistically. Altinbalik and Ayer (Ref 16) employed the upper bound method to define a new kinematically admissible velocity field for extrusion of clover

Amin Seyyed Nosrati, Karen Abrinia, and Ali Parvizi, School of Mechanical Engineering, College of Engineering, University of Tehran, Tehran, Iran. Contact e-mails: a_seyyednosrati@ut.ac.ir, cabrinia@ut.ac.ir, and aliparvizi@ut.ac.ir.

sections. They determined the extrusion loads and material flow for different die inlet and transition geometry combinations. They also introduced the axial deviation of the extruded product as a criterion for determining the quality of the final product. Karami et al. (Ref 17) applied the upper bound method to formulate the deformation geometry for the analysis of non-symmetric extruded sections taking into account the variation of the dead zone size at different angular positions. They also used the curved surfaces to define entry and exit sections of the deforming region. Using the proposed method, the complexity of the exit section was investigated on the extrusion pressure. Venkatesh and Venkatesan (Ref 18) applied area mapping technique to the upper bound method to define deformation zone of extrusion process through the streamlined dies and predict the extrusion force. Using the suggested method, they transformed the bordering points on the surface of initial billet to final section. These authors also calculated the stress and strain distribution at deformation zone. Onlaghi and Assempour (Ref 19) carried out a study based on the upper bound method to determine the radial position of the die holes in an extrusion using a multi-hole die with non-symmetric nature and minimized the exit profile curvature. They used the linear dead metal zone to define the deformation zone. According to this work, the extruded profile curvature was obtained by a deviation function based on the velocity field. Farzad and Ebrahimi (Ref 20) presented a theoretical model using the upper bound method and simulated annealing algorithm to analyze the extrusion process. They proposed a kinematically admissible velocity field and consequently obtained the optimum die profile by minimizing the extrusion load. They also investigated the effect of reduction of area, material work hardening and friction factor on the optimum die profile. Hussein and Kadhim (Ref 21) employed the upper bound method to investigate the extrusion of circular, square, and rhomboidal sections using a continuous velocity field. They used the third- and fifth-degree polynomial functions to define the die surface. In this method, the extrusion pressure and material flow were obtained analytically. Haghghat and Parghazeh (Ref 22) used the upper bound method to give a solution for the problem of the extrusion of strain hardening materials. They also used this method to predict the central bursting defects. The proposed velocity field was used to define the criteria for central cavity formation. They found that the central bursting defects are influenced predominantly by the strain hardening exponent.

However, although in many previous works as discussed above, the analytical investigations on forward extrusion have been carried out, however, one could hardly find any generalized formulation giving a realistic material flow pattern for the forward extrusion process using the upper bound method. In other words, in all previous works the material flow patterns deviate from the physical reality of the problem especially for complicated shaped profiles.

The aim of this study is to present a more realistic analytical solution for the forward extrusion of non-axisymmetric sections using upper bound method which could be applied to real problems. Material flow patterns could easily be predicted by the present method making it easier for the extrusion process engineers to design the process, the dies and toolings required for a successful outcome. New features for this method included the curved streamlines and more accurate definition for material flow in the cross-sectional area. The relative extrusion pressure was determined by minimizing the upper

bound on power utilizing the parameters used in the formulation of the velocity field. Response surface methodology (RSM) with Box-Behnken approach was applied to predict the minimum relative extrusion pressure. The proposed method was validated using experimental and numerical results.

2. Theory

2.1 Geometric Definition of the Deformation Zone

The present study involved applying the upper bound method to analyze the forward extrusion process. New formulation has been developed from previous works by one of the authors (Ref 14, 15, 17, 23, 24). In the proposed method, the variation of dead metal zone (DMZ) length and accordingly changes in the Hermite streamlines were taken into account in order to eliminate the sharp velocity discontinuities at the material flow entry and exit. A simple extrusion of circular to rectangular and L-shaped sections was chosen as a sample to start with, as shown in Fig. 1(a) and (b). It could be seen from Fig. 1(a) and (b) that the material nest area changes at various angles which in turn has an impact on the shape of streamlines. The materials nest area has been utilized to define DMZ. Figure 1(c) and (d) demonstrates the geometry of the deforming regions for the extrusion of rectangular and L-shaped profiles as the cases for three-dimensional non-axisymmetric problems. In both Fig. 1(b) and (d) as indicated the curved surface which is the interface between the billet and the deforming region is shown in three-dimensional view while its two dimensional view is shown in Fig. 1(a) and (c) as a circle. A generic point on a general streamline DD' is defined by the following expression:

$$r(u, q, t) = f(u, q, t)\hat{i} + g(u, q, t)\hat{j} + h(u, q, t)\hat{k} \quad (\text{Eq 1})$$

where f , g , and h determine the positions of x , y , and z coordinates, respectively, and u , q , and t are normalized dimensionless parameters varying between 0 and 1 defining the cylindrical coordinates r , y , and z as follows:

$$u = \frac{r}{R}; \quad q = \frac{\phi}{2\pi}; \quad t = \frac{z}{L_{DZ}}. \quad (\text{Eq 2})$$

where L_{DZ} is the DMZ length as shown in Fig. 1. Any point in the deforming region could be defined by changing the parameters u , q , and t .

2.2 Formulating the Surface of Deforming Region at the Material Entry (Z_1)

Taking into account the changes in the length of DMZ at different angles on the section, the surface of material entry to the deforming region has been defined. A function formulating the DMZ length has been used (Ref 17) here:

$$L_{DZ}(\phi') = L_c \left(1 + \frac{l(\phi')}{R} \right) \quad (\text{Eq 3})$$

where l is the nest of material length at angle ϕ' and L_c is the parameter used for optimizing the upper bound on power. The parameters of Eq 3 are shown in Fig. 1. A fourth-degree polynomial equation has been used to define the discontinuity surface for the material entrance to the deforming region as follows:

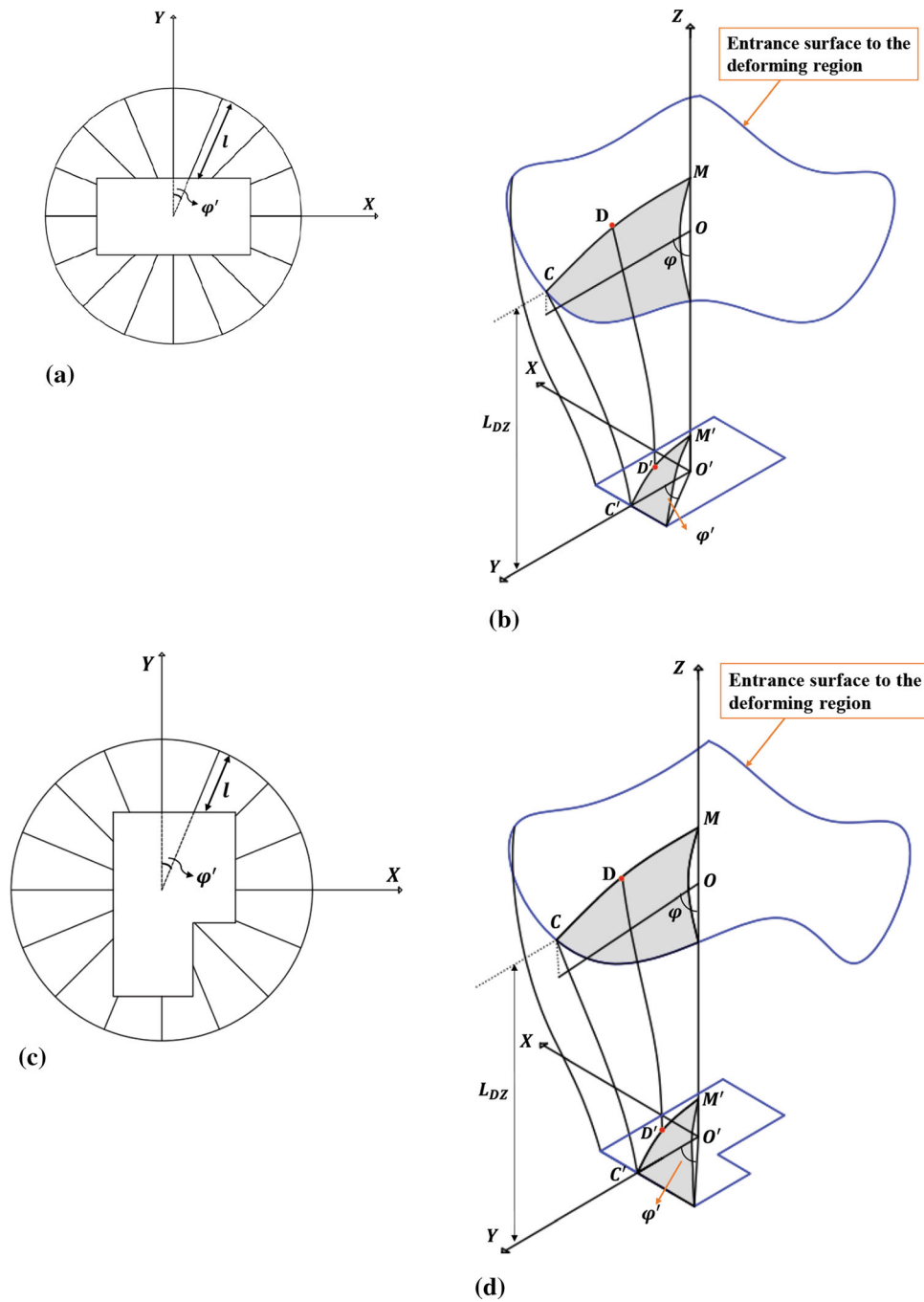


Fig. 1 (a) and (c) Variation of l , (b) and (d) the deforming region geometry for rectangular and L-shaped profiles

$$Z_1 = p_1 + p_2 X_0 + p_3 Y_0 + p_4 X_0^2 + p_5 X_0 Y_0 + p_6 Y_0^2 + p_7 X_0^2 Y_0^2 + p_8 X_0^3 + p_9 Y_0^3 \quad (\text{Eq 4})$$

where

$$\begin{aligned} X_0 &= uR \sin(2\pi q) \\ Y_0 &= uR \cos(2\pi q) \end{aligned} \quad (\text{Eq 5})$$

where $p_1, p_2, p_3, p_4, p_5, p_6, p_7, p_8$ and p_9 are the coefficients in the equation and X_0 and Y_0 are the X and Y coordinates of any

point on the entry surface of deforming region. Function Z_1 has been obtained by fitting a number of points on the discontinuity surface in the entry to the deforming region by using MATLAB Surface Fitting Tool. Surface Z_1 is fitted to the followings:

Point i :

$$P_i = [R \cos(2\pi i/n) \quad R \sin(2\pi i/n) \quad L_{DZ}(2\pi i/n)] \quad i = 1 \text{ to } n$$

Point M :

$$\text{Point } M = [0 \quad 0 \quad O'M]$$

(Eq 6)

where n is the number of points on the surface of discontinuity for the material entry and point M is the center point of the surface. OM is the parameter for minimizing the upper bound on power as shown in Fig. 1. In this paper, rectangular and L-shaped sections have been investigated, and for these, n is equal to 16. Therefore, the position vector defining the discontinuity surface for the material entry to the deforming region is given by:

$$\vec{r}_1 = uR \sin(2\pi q)\vec{i} + uR \cos(2\pi q)\vec{j} + Z_1(u, q)\vec{k} \quad (\text{Eq 7})$$

2.3 Defining the Velocity Discontinuity Surface for the Exit from the Deforming Region (Z_2)

A cubic Bezier function in terms of the parameter u has been used to define the surface of discontinuity for the exit from the deforming region as follows:

$$Z_2(u) = (1-u)^3 P_{0z} + 3u(1-u)^2 P_{1z} + 3u^2(1-u) P_{2z} + u^3 P_{3z} \quad (\text{Eq 8})$$

where P_{1z} and P_{2z} defined controlling points for the curvature and tangents and P_{0z} and P_{3z} were the start and end points for the curve, respectively. Points P_{0z} and P_{1z} must have equal z components to obtain a logical tangent line:

$$P_{0z} = d; P_{1z} = d; P_{2z} = \frac{3d}{4}; P_{3z} = 0 \quad (\text{Eq 9})$$

where d is the parameter for the upper bound optimization. The position vector for the discontinuity surface at the exit from the deforming region could be defined as:

$$\vec{r}_2 = u(O'C' \sin \phi' \vec{i} + O'C' \cos \phi' \vec{j}) + Z_2(u, q)\vec{k} \quad (\text{Eq 10})$$

As shown in Fig. 1, for the given geometry of the extruded product and the extrusion ratio η , the following relations was derived:

$$\begin{aligned} F &= uO'C' \sin \phi' \\ G &= uO'C' \cos \phi' \end{aligned} \quad (\text{Eq 11})$$

2.4 A Realistic Formulation for the Material Flow

Defining a realistic velocity vector for the material and predicting the extrusion pressure accurately requires the correct definition for the material flow. In most previous analytical studies such as (Ref 14, 19), the internal flow pattern for all values of parameter u was in a form following the exact geometry of the exit section and not consistent with the empirical observations. As an example, for an extruded rectangular profile, the material flow pattern remained the same rectangular shape going from the center of the exit cross section toward the profile edges. However, what happens in reality as indicated in the experimental observations (Ref 23, 25) is that the material flow pattern near the center of exit profile is more like the initial billet cross section (circular) and as one gets more closer to the edges of the cross section, it follows the geometry of the exit cross section (e.g., rectangle).

Therefore, based on these empirical observations, it is necessary to formulate the analytical relations in such a way to accommodate for them.

The comparison of the proposed material flow pattern with the previous methods is shown in Fig. 2(a). The modified flow pattern is based on the division of exit cross section into several regions. Figure 2(b) shows the appropriate divisions of the flow pattern for a quarter of square cross section. The exit and entry sections are divided into three parts (see also Fig. 2b). By using the compressibility conditions, each part of the exit section is related to the corresponding part of the entry section (mass conservation). Hence, each part could be formulated individually. Two cubic Bezier curves were used to divide the exit section into three regions as shown in Fig. 2(b).

A cubic Bezier curve is applied to determine the angular changes along the boundary of Region 1 and Region 2 in radial direction. Bezier curve 1 is expressed as:

$$\begin{aligned} q_{L1} &= q_1(1-u)^3 + 3q_{m1}u(1-u)^2 + 3q_{m2}(1-u)u^2 + q_2u^3 \\ q_{m1} &= q_{m2} = q_1 \end{aligned} \quad (\text{Eq 12})$$

where q_1 and q_2 represent the dimensionless angular parameters of $Q'O'Q'$ and $Q'O'R'$, respectively. The curvature and tangents to the curve at controlling points are q_{m1} and q_{m2} , respectively. The angular variations for Region 1 are as follows:

$$q_{R1} = q_1(1-q) + q \cdot q_{L1} \quad (\text{Eq 13})$$

Then, x and y coordinates for any arbitrary point on the section of the extruded profile for Region 1 could be obtained, respectively, by:

$$\begin{aligned} F_1 &= \frac{4u\pi q_{R1} R^2 \eta}{na} \\ G_1 &= \frac{ua}{2} \end{aligned} \quad (\text{Eq 14})$$

Here, u and q are given values between 0 and 1, all points on the Region 1 are defined.

To determine the angular changes along the boundary of Region 2 and Region 3 in the radial direction, Bezier curve 2 is expressed as:

$$\begin{aligned} q_{L2} &= q_3(1-u)^3 + 3q_{m3}u(1-u)^2 + 3q_{m4}(1-u)u^2 + q_2u^3 \\ q_{m3} &= q_{m4} = q_3 \end{aligned} \quad (\text{Eq 15})$$

where q_3 represent the dimensionless angular parameter of $R'O'S'$. The angular variations for Region 3 are as follows:

$$q_{R3} = q_{L2}(1-q) + q \cdot q_3 \quad (\text{Eq 16})$$

Then, for any arbitrary point on the extruded profile section for Region 3, the x and y coordinates could be obtained, respectively, by:

$$\begin{aligned} F_3 &= \frac{ua}{2} \\ G_3 &= u \left(a - \frac{4u\pi q_{R3} R^2 \eta}{na} \right) \end{aligned} \quad (\text{Eq 17})$$

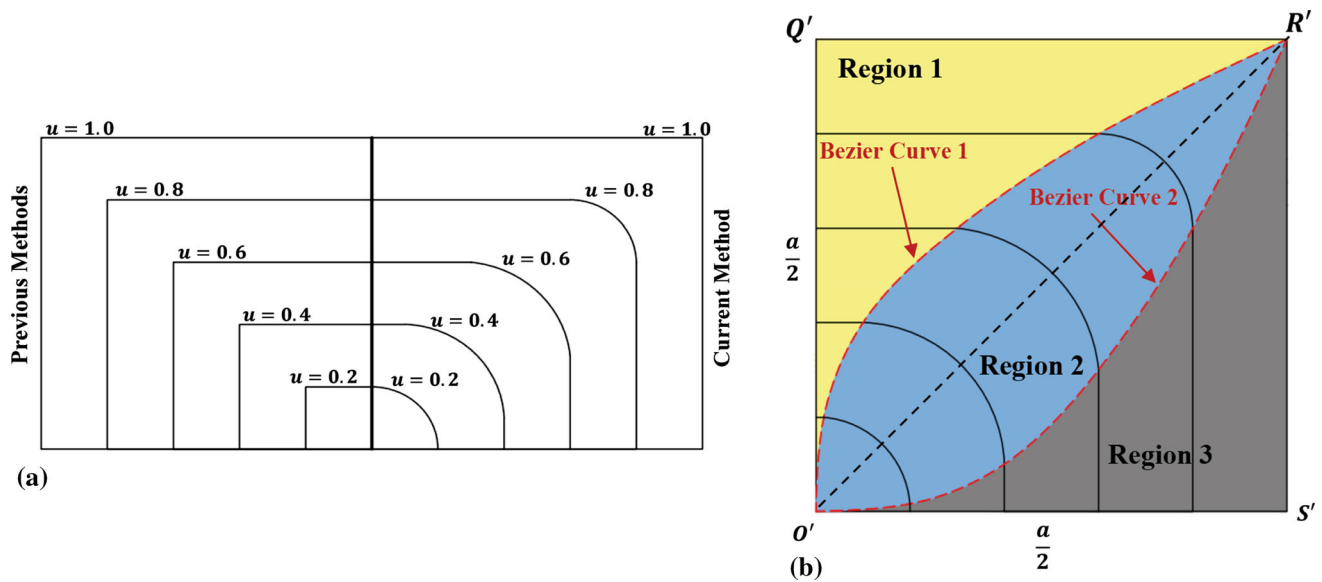


Fig. 2 (a) Schematic material flow pattern comparison of the new formulation and previous methods (Ref 14, 15) and (b) the modified flow pattern for a quarter of square cross section

Using a Bezier curve, any point on the exit section for Region 2 could be defined in Cartesian coordinates consequently as:

$$\begin{aligned} F_2 &= x_1(1 - 2\bar{q}_{R2} + \bar{q}_{R2}^2) + x_m(2\bar{q}_{R2} - 2\bar{q}_{R2}^2) + x_2\bar{q}_{R2}^2 \\ G_2 &= y_1(1 - 2\bar{q}_{R2} + \bar{q}_{R2}^2) + y_m(2\bar{q}_{R2} - 2\bar{q}_{R2}^2) + y_2\bar{q}_{R2}^2 \end{aligned} \quad (\text{Eq 18})$$

where \bar{q}_{R2} is a dimensionless parameter of angular variations for Region 2 given by:

$$\bar{q}_{R2} = \frac{q_{R2} - q_{L1}}{q_{L2} - q_{L1}} \quad (\text{Eq 19})$$

The angular variations for Region 2 are as follows:

$$q_{R2} = q_{L1}(1 - q) + q_{L2} \cdot q \quad (\text{Eq 20})$$

x_1, y_1 and x_2, y_2 represent the position of any point on Bezier curve 1 and Bezier curve 2, respectively, given by:

$$\begin{aligned} x_1 &= \frac{4u\pi q_{L1} R^2 \eta}{na} \\ y_1 &= \frac{ua}{2} \\ x_2 &= \frac{ua}{2} \\ y_2 &= u \left(a - \frac{4u\pi q_{L2} R^2 \eta}{na} \right) \end{aligned} \quad (\text{Eq 21})$$

x_m, y_m are the positions of controlling points in Region 2 given by:

$$\begin{aligned} x_m &= \frac{x_1 + k_0 x_2}{k_0 + 1} \\ y_m &= \frac{k_0 y_1 + y_2}{k_0 + 1} \end{aligned} \quad (\text{Eq 22})$$

k_0 is the optimization parameter used in the upper bound method.

2.5 Streamlines

Using a cubic parametric Hermite function, the material flow path is formulated in the deforming region. The velocity discontinuities could be eliminated for the material entrance and exit to the deforming region by equating the X - and Y -components of the start and end points of the tangent vectors \vec{r}'_1 and \vec{r}'_2 , to zero. As a result, the position vector of any arbitrary point is given by:

$$\begin{aligned} \vec{r} &= f(u, q, t)\hat{i} + g(u, q, t)\hat{j} + h(u, q, t)\hat{k} \\ &= [1 - 3t^2 + 2t^3 \quad 3t^2 - 2t^3 \quad t - 2t^2 + t^3 \quad -t^2 + t^3] \\ &\quad \times \begin{bmatrix} uR \sin(2\pi q) & uR \cos(2\pi q) & Z_1 & Z_2 \\ F & G & C_1 L_c + uL_c & -C_2 L_c - uL_c \end{bmatrix} \times \begin{bmatrix} \vec{i} \\ \vec{j} \\ \vec{k} \end{bmatrix} \end{aligned} \quad (\text{Eq 23})$$

C_1 and C_2 are the optimization parameters that would be used for upper bound computations.

The kinematically admissible velocity field is obtained according to "Appendix 1." To identify an accurate velocity field, calculations were performed to optimize the upper bound on the total power consumption and from that the extrusion pressure was calculated (see "Appendix 2"). To illustrate further, the capabilities of the present method and to support the claim made earlier that it is comparable to finite element method, producing similar results here are given details about the strain values in the deforming material. The effective strain is obtained using the formulations given in "Appendix 3."

3. Experiments

Physical modeling experiments with plasticine have been applied to validate the analytical results. The experimental investigations were carried out for the extrusion of rectangular and L-shaped sections from a circular billet using flat-face dies.

The material used for the tooling was Plexiglas (Fig. 3a). In order to observe the material flow pattern after deformation, five contrasting colors of plasticine were used to prepare the billets in the forms of concentric cylinders as shown in Fig. 3(b). The reductions of area for the extrusion of rectangular and L-shaped profiles were 80% and 70%, respectively. The height and diameter of the billets were 60 mm and 44 mm, respectively. The press velocity was set to 2 mm per minute in order to have a quasi-static condition. An Instron 4028 hydraulic press was used to carry out the experiments (Fig. 3c). Uniaxial compression tests were carried out on plasticine sample 44 mm in high and 44 mm diameter, to obtain stress-strain relation. Tests were conducted at strain rate of 0.01 s^{-1} at room temperature. The strain range for these tests was 0-0.7. The experimental stress-strain relation was obtained for the material as follows:

$$\bar{\sigma}(\text{MPa}) = 0.06 + 0.13(\bar{\epsilon})^{0.15} \quad (\text{Eq 24})$$

This relationship was used for the FEM analysis.

The uniaxial yield strength of 0.06 MPa for plasticine was determined from a compression test. The compression ring tests were performed to determine friction factors, using lubricant Vaseline. The friction factor, $m = 0.2$, was obtained which was in agreement with the value obtained from previous study (Ref 26, 27). Details for the rectangular and L-shaped sections are displayed in Fig. 3(d). The final extruded products were cut along their cross section to inspect the material flow pattern.

4. FEM Simulation

Physical modeling experiments were carried out to support the finite element simulation. DEFORM™ 3D commercial software was applied to simulate the extrusion process. Rigid

body model was used for the die and punch, but a deformable solid model was assumed for the billet. The billet was meshed with 70,000, tetrahedral elements. The mesh sensitivity was checked to make sure that the correct number of elements has been chosen. The model's dimensions and simulation conditions were taken similar to the experiments. A punch velocity of 1 mm/s was applied. Since the behavior of plasticine at ambient temperature in the deformation process is similar to that of metals such as steel at high temperature, the coefficient of heat exchange between the material and the tool was considered to be $11 \text{ N}/(\text{mm s}^\circ\text{C})$ (Ref 27). The coefficient of heat exchange between the billet and the air was $0.02 \text{ N}/(\text{mm s}^\circ\text{C})$ according to mentioned reason. Equation 24 was used to define the flow stress. A typical view of the extruded L-shaped profile is shown in Fig. 4.

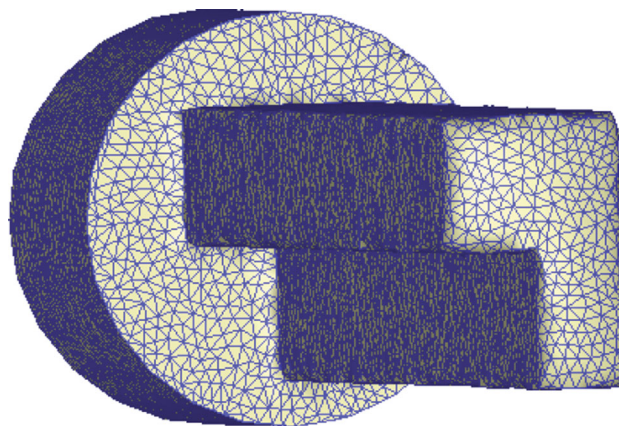


Fig. 4 Deformed finite element model of the L-shaped section

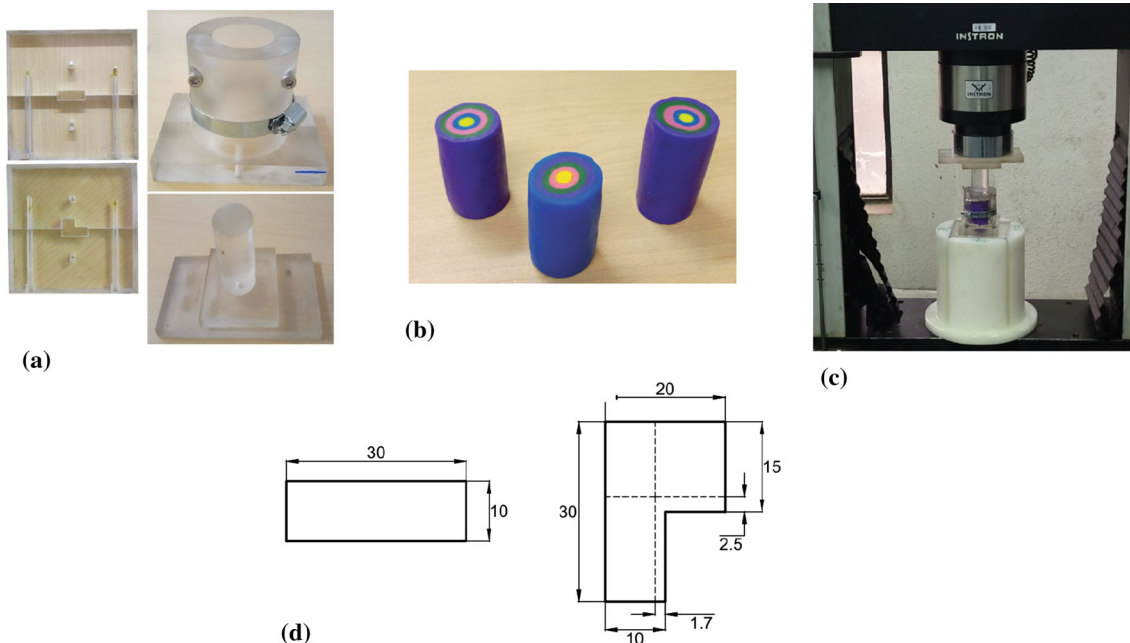


Fig. 3 (a) The tooling, (b) the billets, (c) the experimental setup and (d) details of the extruded profile shapes used for the tests (all dimensions in mm)

Table 1 Optimization results of the upper bound solution

	P/Y	C_1	C_2	\bar{d}	\bar{L}_c	\overline{OM}	k_0
L-shaped profile	2.70	- 1	- 0.5	0.18	0.18	1.12	60.72
Rectangular profile	3.40	- 1	- 1	0.13	0.20	0.91	40.28

Table 2 Comparison of upper bound, finite element and experimental results for the forward extrusion of rectangular and L-shaped sections

	Rectangular profile	L-shaped profile
Upper bound method	3.40	2.70
Experiment	3.35	2.46
FEM	3.30	2.67

5. Results and Discussion

5.1 The Solution Given by the New Formulation

Using the formulation given in Sect. 2 of this paper, a generalized solution was given for the forward extrusion of shaped profiles. This method of analysis was applied for two profiles: rectangular and L-shaped sections. These shapes were chosen only as samples and the method could be applied to the extrusion of many other profiles as well. In the present formulation, six parameters (\bar{L}_c , \overline{OM} , C_1 , C_2 , \bar{d} and K_0) relating to the streamlines and the velocity field were incorporated. \bar{L}_c , \bar{d} and \overline{OM} are the dimensionless parameters given as follows:

$$\bar{L}_c = \frac{L_c}{R}; \quad \bar{d} = \frac{d}{R}; \quad \overline{OM} = \frac{OM}{R} \quad (\text{Eq 25})$$

Hence, the computation based on upper bound which requires a minimization process was carried out. Utilizing these parameters was necessary since it helped to shape the streamlines and hence the velocity field in such a way as to approach the actual physical reality. This was shown to be true by obtaining a lower upper bound on extrusion pressure as compared with previous results and verified by experimental and FEM data. This means that by changing the above-mentioned parameters, the value of extrusion pressures is aimed to become minimum while changing the shapes of the streamlines and stream surface automatically to push the velocity field closer to the actual one in the problem.

5.2 Optimization

In this study, the optimization objective was to minimize the upper bound on power and consequently the pressure. The desirability approach was used to perform the optimization process. Table 1 presents the optimization results of the upper bound solution for the L-shaped and rectangular profiles. It could be observed from Table 1 that the minimum relative extrusion pressures for L-shaped and rectangular profiles are 2.70 and 3.40, respectively. Furthermore, at these minimum relative extrusion pressures, the die length parameter (\bar{L}_c) for L-

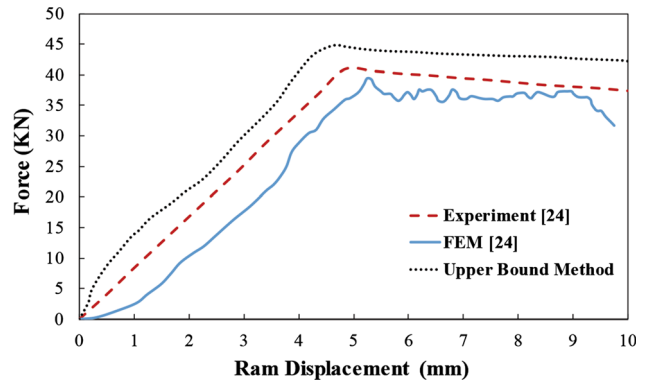


Fig. 5 Upper bound method, FEM, and experimental force-displacement curves for extrusion of square section for 60% reduction of area ($m = 1$)

shaped profile and rectangular profile is 0.18 and 0.20, respectively. The decrease in relative extrusion pressure and length of the die is due to the lower reductions of area in extrusion of L-shaped profile relative to rectangular profile (Ref 14).

To verify the results of the proposed method, the experimental tests and finite element analysis were performed. Table 2 shows the results of upper bound and finite element methods along with the experimental data. The finite element results are below, and the upper bound data are above the experimental results. The differences between these results are also demonstrated in Table 3. It is obvious that the upper bound results for rectangular section are close to the experimental results. However, for the L-shaped profile, differences between the upper bound and experimental results are higher. This could be due to the complexity of the L-shaped section and inhomogeneous metal flow. It should be noted that the complexity of the extrusion section is defined in different ways by the researchers. In general, the greater the stress concentration and corner locations in a section, the greater the degree of complexity and thus the higher inhomogeneity during the deformation process. This increases the pressure required for the process (Ref 28). In this study, the L-shaped section is more complex than the rectangular one because it has more stress concentration locations. The proposed method could also be used to analyze more complex sections, such as T and I . The accuracy of the upper bound analysis depends on the formulation of the admissible velocity field and its closeness to the real physical situation. Therefore, if the proposed admissible velocity field is not close enough to the real case then much less accurate results are obtained. Although the numerical methods may provide close answers to experimental results for extrusion of more complex sections, these methods require a long process to obtain results and they consume more CPU time meaning

Table 3 Percentage difference between upper bound, finite element and experimental results for the forward extrusion of rectangular and L-shaped sections

	Rectangular section	L-shaped section
% Difference between UB and Exp	1.5	9.7
% Difference between FEM and Exp	1.5	8.5

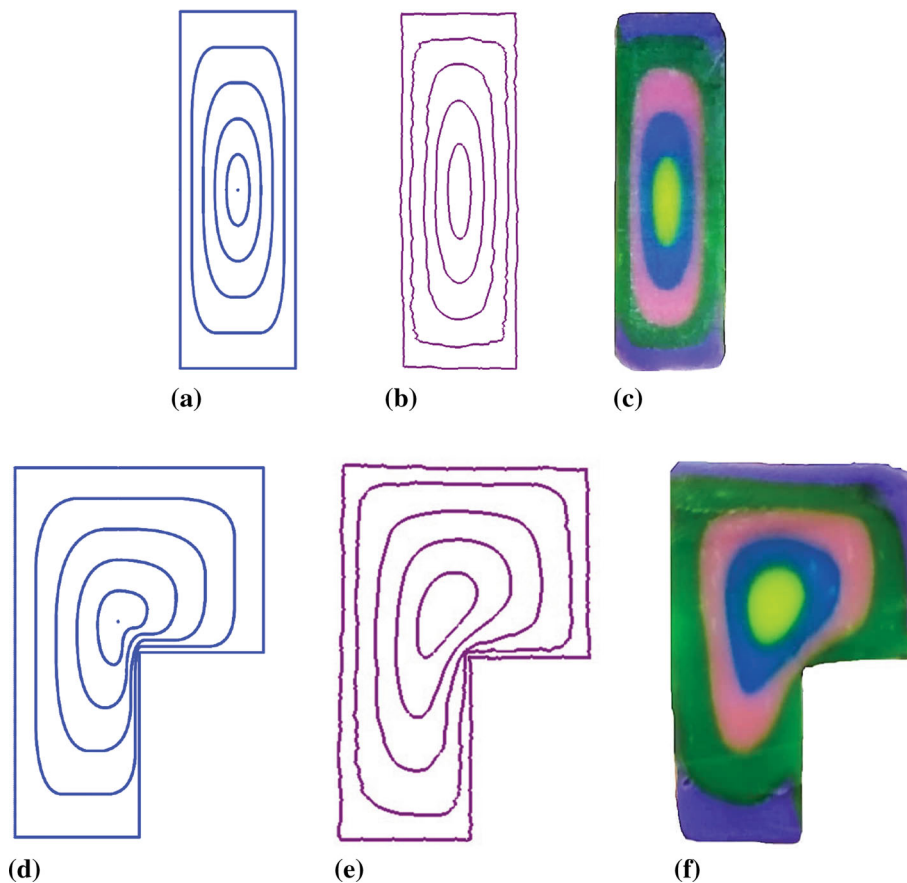


Fig. 6 Internal material flow pattern for extrusion of rectangular and L-shaped profile, (a) and (d) analytical, (b) and (e) FEM, (c) and (f) experiment

more time and expense. In addition, unlike the upper bound method, the optimal solution to the problem is not obtained by numerical methods, and simulations are often performed for a given condition. However, simulation for different conditions can be done by employing an iterating loop, but it will be very time-consuming and sometimes inefficient.

As further evidence for the agreement between the results obtained from the present method with experimental data, the force-displacement curves obtained from the FEM and experimental results for a lead alloy (Ref 24) were compared with the curve from the proposed method in Fig. 5. As depicted from the figure, the results for the extrusion force display good agreements. The extrusion force rises until it reaches a pick value, i.e., steady state position for the extrusion process, and then, it is slightly reduced due to the lower interface frictional power (i.e., contact length reduces) between the container and the billet.

5.3 Material Flow

The cross-sectional material flow patterns obtained from the proposed upper bound method are compared with those from experimental and finite element study in Fig. 6. It is seen from Fig. 6 that at the center of exit profile, i.e., for smaller u -values, the flow pattern is similar to that of the initial billet section contour due to the low strain experienced during the deformation process. In contrast, at the boundary areas of the profile, i.e., for the higher u -values, are more deformed and subjected to higher strains, forming the final output profile. This proposed method eliminated the unreal discontinuities existed in previous definitions of material flow and provided a more realistic prediction for the deformation during the forward extrusion process. In most previous works (such as Ref 29, 30), all the contours with the same u -values in the deforming region changed from the shape of the initial billet pattern to the final

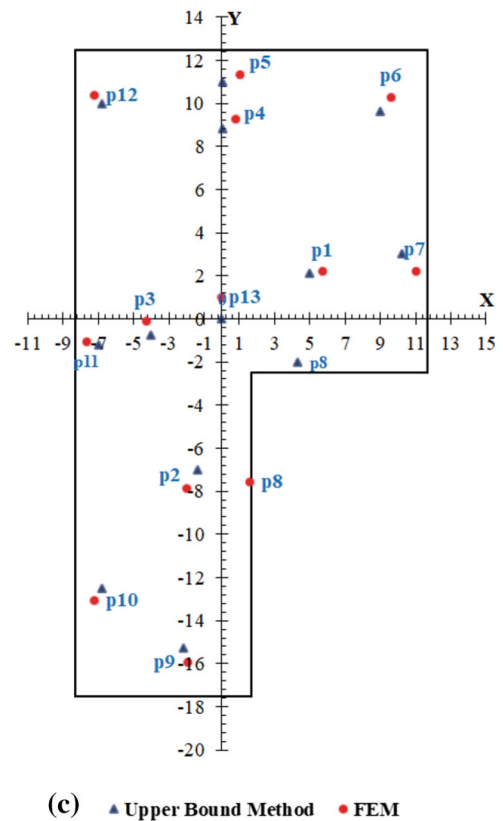
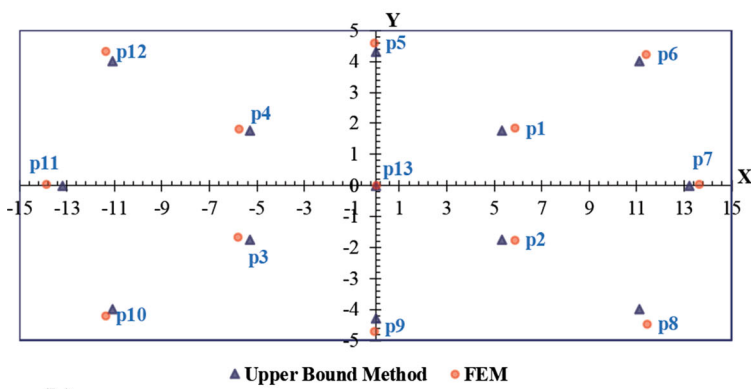
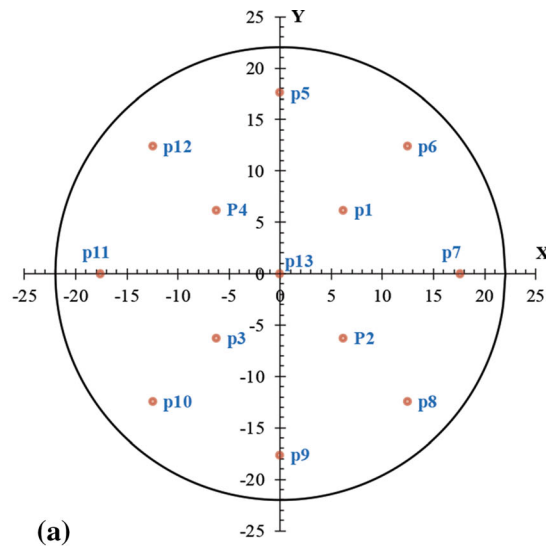


Fig. 7 (a) The initial position of the points in the billet cross section, analytical and FEM results of point tracking for (b) rectangular profile and (c) L-Shaped profile

Table 4 The relative error for point tracking results

	Rectangular profile	L-shaped profile
RE (%)	11	17

section contours as the billet advanced through the deforming region. Material flow contours predicted by the present method and obtained from experiments and finite element simulation

show close agreements as shown in Fig. 6. To compare the analytical and numerical results of the internal material flow quantitatively, the point tracking method was employed for the extrusion of rectangular and L-shaped profile. Thirteen points with the same z-value were considered on the cross section of the initial billet as shown in Fig. 7(a). The positions of the considered points on the cross section of the final profile after the analytical and numerical analysis for the extrusion of the rectangular and L-shaped profile are displayed in Fig. 7(b) and (c), respectively. The relative error (RE) was defined to express the nonuniformity of the deviation as follows:

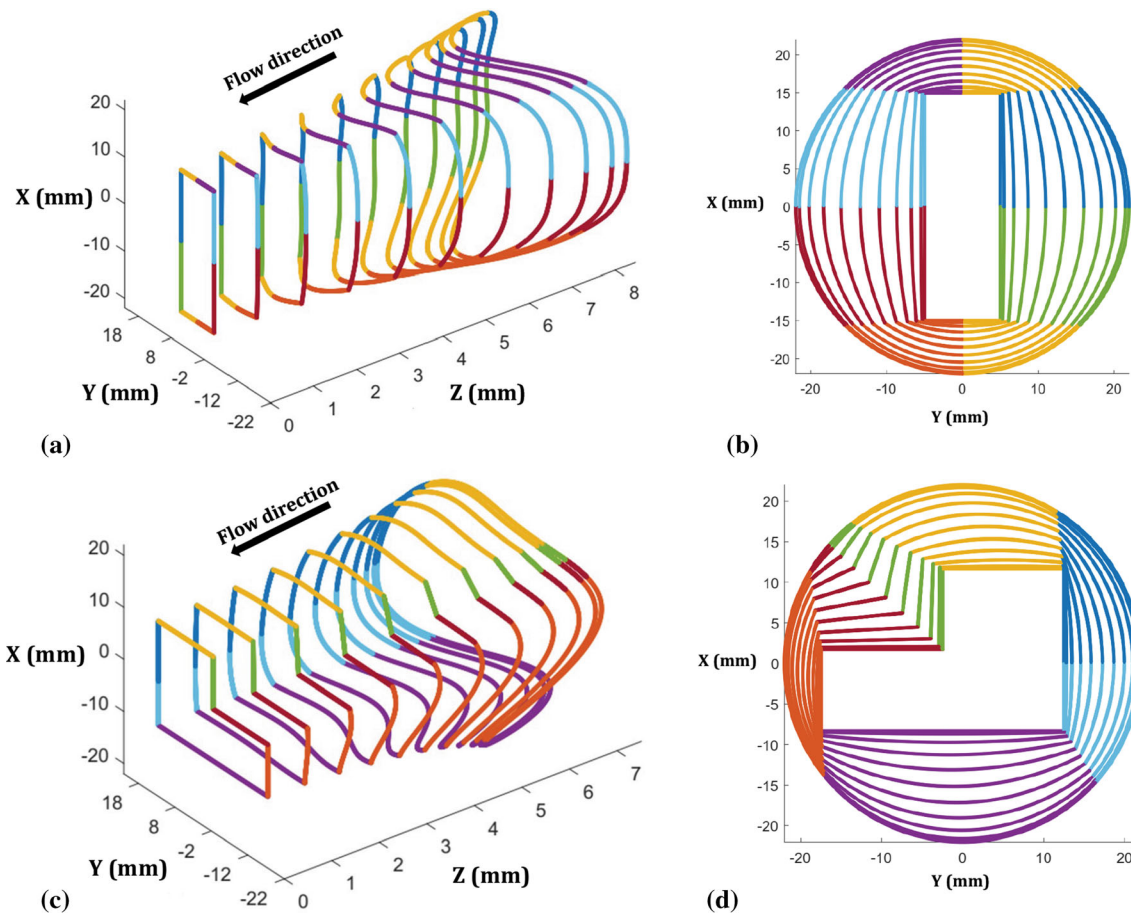


Fig. 8 The deforming zone geometry for the extrusion of rectangular and L-shaped profiles; (a) and (c) 3D view, (b) and (d) 2D view

$$RE = \frac{\sum_{i=1}^n |(f_i - u_i)/f_i|}{n} \times 100\% \quad (\text{Eq 26})$$

where f_i is the value of the finite element method; u_i is the predicted data from the upper bound method and n is the number of points. Table 4 gives the standard errors of the average positions of the points. By comparing the average difference in positions of points for the analytical and numerical method, it could be observed that the relative error for the positions of points for the rectangular and L-shaped profile are 11% and 17%, respectively, which are within the acceptable limits. This information indicates that the analytical results for the internal material flow are consistent with the finite element results.

It should be said that the analytical solution based on the upper bound method is obtained very rapidly in a matter of few minutes while the numerical results using FEM are obtained taking moderately long procedures for deformation processes, they consume a lot of CPU time meaning more time and expense. In this study, the time taken for each finite element simulation was up to 17 h while the time taken for upper bound method was less than 30 min. On the other hand, in finite element simulations, a new modeling and solving processes is needed to solve each and every new problem with a specific geometry, which increases the time required to solve the problem while in the analytical method by changing the geometry or a process parameter it takes only minutes to reach

the same results. It is concluded that further time and money have to be consumed for FEM numerical simulation while with the analytical method proposed in this study, any change in the geometry could be applied very rapidly and simply hence saving much time and money. To illuminate this statement more, keep in mind that analysis of the extrusion process must be done under different conditions such as different die profiles and friction factors. In the FEM analysis for each different die profile and friction factor, all the procedures of preprocessing, processing and post-processing must be repeated every time while with the proposed analytical solution, all of these changes could be performed in a more time efficient way.

In order to understand the dead metal zone formation and to demonstrate the inhomogeneity of material flow, geometry of the deformation zone is presented in Fig. 8 for different values of parameter t for the extrusion of rectangular and L-shaped profiles. As indicated in Fig. 8, the streamlines in $x - y$ plane at the entrance of the deforming region ($t = 0$) have a circular shape and take the shape of the final profile while advancing toward the exit in the deforming region. For each profile, the optimum value of length L_c which is an indication of the length of the deformation zone along the Z-axis increases for higher values of the reduction of area (see Table 1). It has been said that the optimum value of $\overline{L_c}$ is influenced by the shape complexity. Higher optimum $\overline{L_c}$ is obtained for more complex profiles due to more inhomogeneous metal flow (Ref 17). The results in Figs. 6, 7 and 8 demonstrate the robustness of the proposed method for the analysis of the forward extrusion

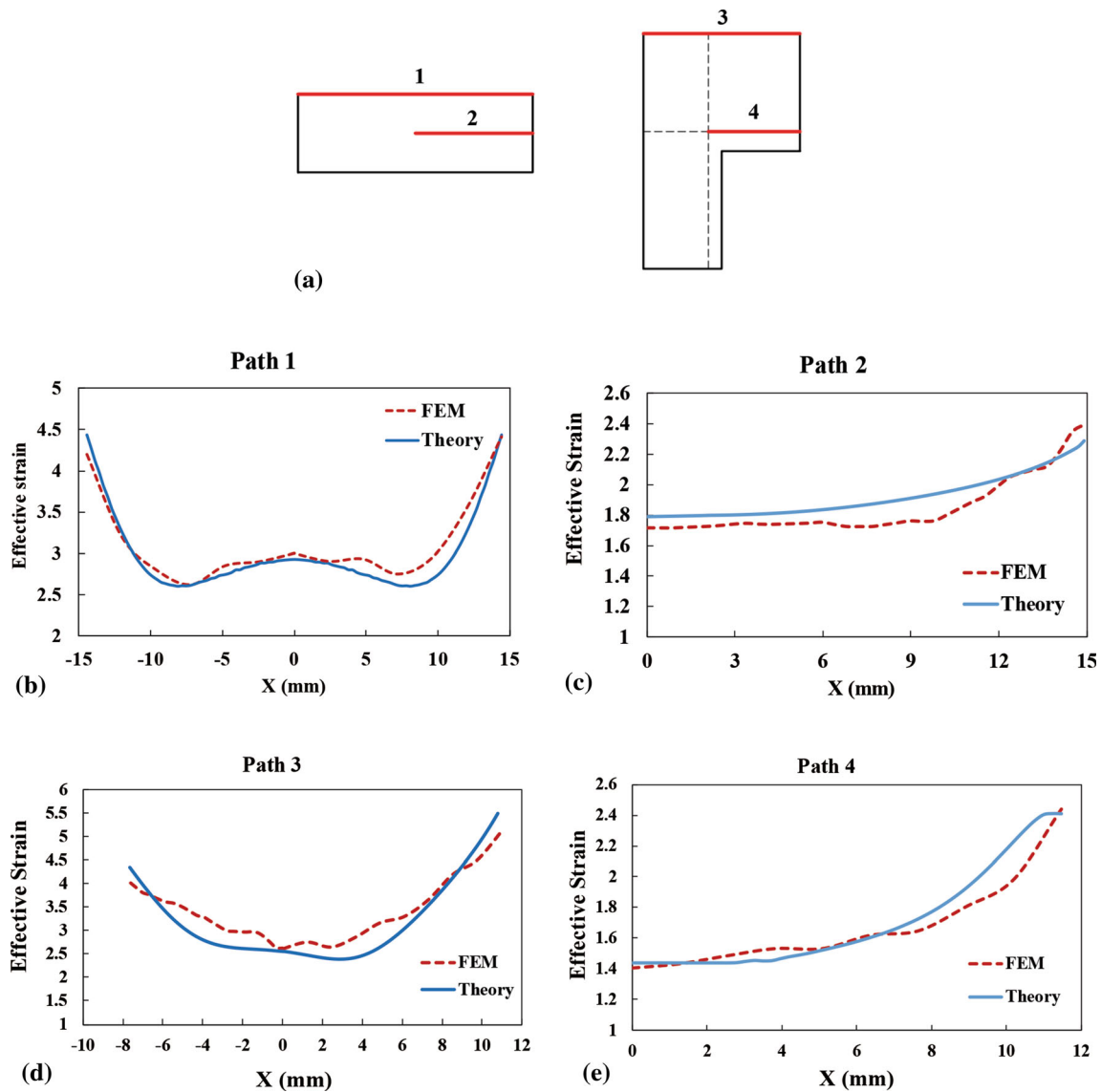


Fig. 9 (a) Path lines on the exit surfaces of profiles; strain distribution along path lines of (b), (c) rectangular and (d), (e) L-shaped sections ($m = 0.2$)

process, which could realistically predict the internal flow of materials and the geometry of the deformation region.

5.4 Strain Distribution

The strain distribution at the exit section of the extruded product was obtained based on the proposed analytical formulation. The comparison between analytical and numerical distribution of strains at the exit surface of the extruded profiles along some special path lines is demonstrated in Fig. 9. The path lines are presented in Fig. 9(a). This figure reveals that the distribution of strain obtained from analytical solution is in good agreement with numerical results. It could be observed that the amount of strain is the highest value in the corners of the exit sections (Fig. 9b and d). As previously mentioned, the initial billet must undergo more plastic deformation on the edges of the die to form the final shape of the product. In fact, by increasing the distance from the center of the die, the plastic deformation becomes larger and reaches the maximum value in the corners of the die. Increasing plastic deformation will

increase the effective strain. The amount of strain increases as one gets further away from the die center. The higher strain values seen in the corners of the L-shaped section as compared with the rectangular profile are due to the complexity of the final extrusion profile. At these positions, the material flow experiences more hindrance. In addition, the results of the analytical solution reveal that the amount of strain in the center of the die is the smallest value which is shown in Fig. 9c and e. This is due to the occurrence of less plastic deformation in the center of the die, which despite the faster flow of materials, the duration of the material in the deformation region is less and travels less distance.

5.5 Comparison with Previous Works

In order to demonstrate the more realistic definition for the deformation zone, the material flow and the reduced upper bound value and presenting a more clear picture of the capabilities of the present method, the influence of the reduction of area on the relative extrusion pressure for

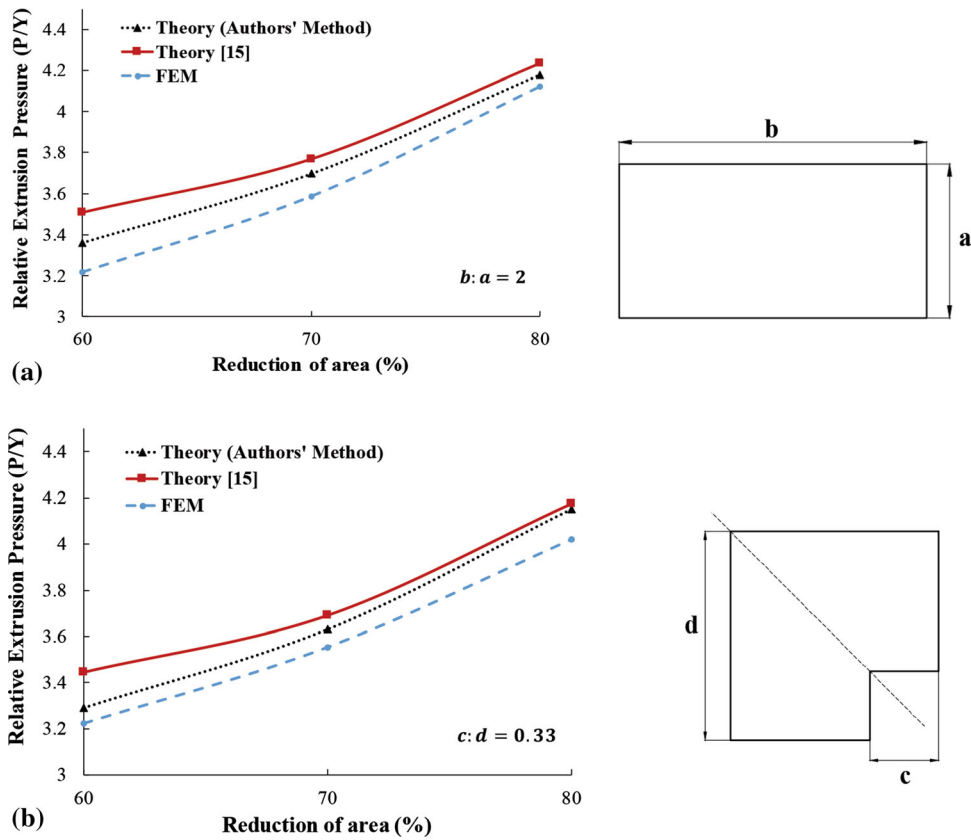


Fig. 10 Influence of the reduction of area on the extrusion pressure ($m = 1$) for: (a) rectangular profile and (b) symmetrical L-shaped profile

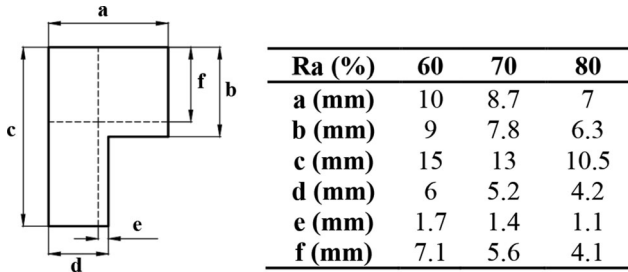


Fig. 11 Dimensions of the L-shaped profiles used for comparison of results

rectangular and L-shaped profiles were investigated as shown in Fig. 10. For the sake of comparison, the frictional conditions used in the finite element simulation were kept similar to the analytical method. It could be observed from Fig. 10(a) and (b) that for higher values of the reduction of area, the extrusion pressure increases; and for each reduction, the proposed method gives better upper bounds which are also closer to the FEM results. It is clear from the figures that the solution based on previous method predicts higher upper bound values.

To validate further the proposed analytical method, experimental and analytical data from previous works have been used for comparison. Figure 11 shows the actual dimensions for the geometry used in this work. Figure 12 gives a comparison for the presented theoretical method, the experiments (Ref 14) and also the previous work for three different

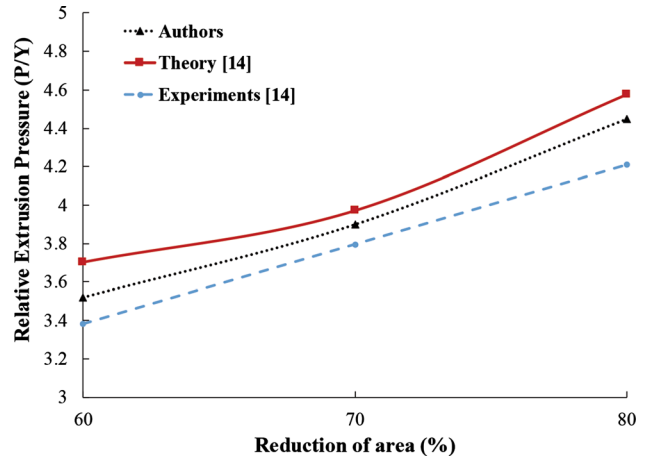


Fig. 12 Comparison of authors results with experimental and previous work for the extrusion of L-shaped profile ($m = 1$)

values of reduction of area for the extrusion of L-shaped profile. Based on the experimental results, for 60%, 70% and 80% of reduction of areas, the values for the relative extrusion pressure are 3.38, 3.78 and 4.19, respectively. For 60%, 70% and 80% reductions of area, the differences between the results given in Ref 14 with the experimental data are 8.7%, 4.4% and 9.5%, while for the present method, they are 3.9%, 3% and 5.8%. According to Fig. 12, the proposed theoretical results are closer to the experimental data than the previous work.

6. Conclusion

A new analytical formulation based on the upper bound theorem was developed to assist process engineers in the extrusion industry to tackle the problem of forward metal extrusion for non-axisymmetric sections such as rectangle and L-shape profiles. The followings could be noted:

- The proposed method facilitates the process, die and tooling design for the engineers in the extrusion industry by giving them the ability to predict the material flow for almost any kind of deforming region.
- The formulation given here predicted the upper bound on pressure and the internal material flow for the extrusion of the shaped sections in a more realistic fashion as compared to previous works.
- The present definition for the velocity field, extrusion pressure and the geometry of the deforming region is more accurate than all the previous works.
- The results computed using the proposed method are found to be close with those obtained experimentally and numerically.
- The present formulation is a robust tool comparable to FEM as much as it could provide all the results such as strain and stress distributions, material flow patterns, pressure and force predictions in exactly the same fashion as FEM, but with less expense and time. Unlike the FEM, it is not able to analyze phenomena such as crack formation, microstructural evolution and tool wear in the extrusion process.

Acknowledgments

The authors are grateful for the research support of the Iran National Science Foundation (INSF) (Grant Number 89003323).

Appendix 1

Velocity Field

A kinematically admissible velocity field was obtained as:

$$V_x = \frac{f_t}{h_t} V_z \quad V_y = \frac{g_t}{h_t} V_z \quad V_z = M(u, q, t) \quad (\text{Eq A.1})$$

where f_t , g_t and h_t are the first derivatives of f , g and h with respect to t . $M(u, q, t)$ is an unknown function satisfied the incompressibility conditions expressed below:

$$\frac{\partial V_x}{\partial X} + \frac{\partial V_y}{\partial Y} + \frac{\partial V_z}{\partial Z} = 0 \quad (\text{Eq A.2})$$

Considering $\left(\frac{\partial V_i}{\partial X_k} = \sum_{j=1}^3 \left(\frac{\partial V_i}{\partial U_j} \right) \cdot \left(\frac{\partial U_j}{\partial X_k} \right) \right)$,

function $M(u, q, t)$ is found by replacing Eq (A.1) into (A.2) as follows (for details see (Ref 14)):

$$M = \frac{C(u, q) \cdot h_t}{h_t(f_u g_q - f_q g_u) + h_q(f_i g_u - f_u g_t) + h_u(f_q g_t - f_t g_q)} \quad (\text{Eq A.3})$$

where C is obtained from the boundary conditions of the problem and is given by:

$$C(u, q) = \left[(f_u g_q - f_q g_u) + h_q/h_t(f_i g_u - f_u g_t) + h_u/h_t(f_q g_t - f_t g_q) \right]_{t=0} \quad (\text{Eq A.4})$$

Appendix 2

The Upper Bound Solution

The upper bound on the total power consumption was presented as:

$$J^* = \dot{W}_i + \dot{W}_e + \dot{W}_x + \dot{W}_f \quad (\text{Eq B.1})$$

\dot{W}_i is the power due to plastic deformation and may be defined as follows:

$$\dot{W}_i = \bar{\sigma} \int_V \dot{\epsilon} dV = \frac{2\bar{\sigma}}{\sqrt{3}} \int_0^1 \int_0^1 \int_0^1 \left(\left(\frac{\dot{\epsilon}_{xx}^2 + \dot{\epsilon}_{yy}^2 + \dot{\epsilon}_{zz}^2}{2} \right) + \dot{\epsilon}_{xy}^2 + \dot{\epsilon}_{yz}^2 + \dot{\epsilon}_{zx}^2 \right)^{1/2} \det J \partial u \partial q \partial t \quad (\text{Eq B.2})$$

where $\dot{\epsilon}_{xx} \dots$ are strain rate components in various directions, $\bar{\sigma}$ is the flow stress and J is the Jacobian for the transformation of coordinates from x, y, z to u, q, z .

\dot{W}_f , the power due to the friction at the die surface and was defined as:

$$\begin{aligned} \dot{W}_f &= \frac{m\bar{\sigma}}{\sqrt{3}} \iint_S \Delta V_f dS_f \\ &= \frac{m\bar{\sigma}}{\sqrt{3}} \int_0^1 \int_0^1 \sqrt{V_x^2 + V_y^2 + V_z^2} \sec \alpha \frac{\partial(x, z)}{\partial(q, t)} \Big|_{u=1} dq dt \end{aligned} \quad (\text{Eq B.3})$$

where $\sec \alpha = \sqrt{(N_1^2 + N_2^2 + N_3^2)/N_2}$ and $N = (\partial r / \partial q)_{u=1} (\partial r / \partial t)_{u=1}$ and m is the friction factor.

\dot{W}_e and \dot{W}_x , the powers due to velocity discontinuities at entry and exit surfaces, respectively, are 0 since there are no velocity discontinuities at the entry and exit boundaries. Having found all the power components, the relative extrusion pressure was computed as follows:

$$P/Y = \frac{J^*}{\pi R^2 v_0} \quad (\text{Eq B.4})$$

where v_0 was the velocity for the initial billet.

Appendix 3

Strain Values Computation

The strain rates components are defined as follows:

$$\begin{aligned}
\dot{\epsilon}_{xx} &= \frac{\partial V_x}{\partial x} \\
\dot{\epsilon}_{yy} &= \frac{\partial V_y}{\partial y} \\
\dot{\epsilon}_{zz} &= \frac{\partial V_z}{\partial z} \\
\dot{\epsilon}_{xy} &= \frac{1}{2} \left(\frac{\partial V_x}{\partial y} + \frac{\partial V_y}{\partial x} \right) \\
\dot{\epsilon}_{xz} &= \frac{1}{2} \left(\frac{\partial V_x}{\partial z} + \frac{\partial V_z}{\partial x} \right) \\
\dot{\epsilon}_{yz} &= \frac{1}{2} \left(\frac{\partial V_y}{\partial z} + \frac{\partial V_z}{\partial y} \right)
\end{aligned} \tag{Eq C.1}$$

The effective strain is obtained by integrating strain rate with respect to time as follows:

$$\epsilon = \int_0^T \dot{\epsilon}_{ef} dt \tag{Eq C.2}$$

where $\dot{\epsilon}_{ef}$ is the effective strain rate which is obtained by:

$$\dot{\epsilon}_{ef} = \left(\left(\dot{\epsilon}_{xx}^2 + \dot{\epsilon}_{yy}^2 + \dot{\epsilon}_{zz}^2 \right) + \frac{1}{2} \left(\dot{\epsilon}_{xy}^2 + \dot{\epsilon}_{yz}^2 + \dot{\epsilon}_{zx}^2 \right) \right)^{1/2} \tag{Eq C.3}$$

And T is the time that a particle travels along the flowlines in the deformation zone. T is obtained as follows:

$$T = \frac{\partial s}{V} \tag{Eq C.4}$$

where

$$\partial s = \left(\partial f^2 + \partial g^2 + \partial h^2 \right)^{1/2} \tag{Eq C.5}$$

$$V = \left(V_x^2 + V_y^2 + V_z^2 \right)^{1/2} \tag{Eq C.6}$$

Clearly once the strain values are known similar to finite element method, stress values could then be derived from the stress strain relations for a particular material.

References

1. S. Bingöl, Ö. Ayer, and T. Altınbalık, Extrusion Load Prediction of Gear-Like Profile for Different Die Geometries Using ANN and FEM with Experimental Verification, *Int. J. Adv. Manuf. Technol.*, 2015, **76**(5–8), p 983–992
2. D.-C. Chen, S.-K. Syu, C.-H. Wu, and S.-K. Lin, Investigation into Cold Extrusion of Aluminum Billets Using Three-Dimensional Finite Element Method, *J. Mater. Process. Technol.*, 2007, **192**, p 188–193
3. H.G. Hosseinabadi and S. Serajzadeh, Hot Extrusion Process Modeling Using a Coupled Upper Bound-Finite Element Method, *J. Manuf. Process.*, 2014, **16**(2), p 233–240
4. F. Li, S.J. Yuan, G. Liu, and Z.B. He, Research of Metal Flow Behavior During Extrusion with Active Friction, *J. Mater. Eng. Perform.*, 2008, **17**(1), p 7–14
5. D. Wang, C. Zhang, C. Wang, G. Zhao, L. Chen, and W. Sun, Application and Analysis of Spread Die and Flat Container in the Extrusion of a Large-Size, Hollow, and Flat-Wide Aluminum Alloy Profile, *Int. J. Adv. Manuf. Technol.*, 2018, **94**(9–12), p 4247–4263
6. J.-Y. Pan and X. Xue, Numerical Investigation of an Arc Inlet Structure Extrusion Die for Large Hollow Sections, *Int. J. Mater. Form.*, 2018, **11**(3), p 405–416
7. Y. Sun, Q. Chen, and W. Sun, Numerical Simulation of Extrusion Process and Die Structure Optimization for a Complex Magnesium Doorframe, *Int. J. Adv. Manuf. Technol.*, 2015, **80**(1–4), p 495–506
8. S. Elgeti, M. Probst, C. Windeck, M. Behr, W. Michaeli, and C. Hopmann, Numerical Shape Optimization as an Approach to Extrusion Die Design, *Finite Elem. Anal. Des.*, 2012, **61**, p 35–43
9. S. Hosseini, M. Sedighi, and J. Mosayebnezhad, Numerical and Experimental Investigation of Central Cavity Formation in Aluminum During Forward Extrusion Process, *J. Mech. Sci. Technol.*, 2016, **30**(5), p 1951–1956
10. M.-S. Joun, M.-C. Kim, D.-J. Yoon, H.-J. Choi, Y.-H. Son, Finite Element Analysis of Central Bursting Defects Occurring in Cold Forward Extrusion, in *ASME 2011 International Manufacturing Science and Engineering Conference, 2011, American Society of Mechanical Engineers Digital Collection*, pp. 169–174
11. W. Johnson and P.B. Mellor, *Engineering Plasticity*, Horwood, Devon, 1983
12. N. Chitkara and K. Celik, Extrusion of Non-symmetric T-Shaped Sections, an Analysis and Some Experiments, *Int. J. Mech. Sci.*, 2001, **43**(12), p 2961–2987
13. J. Ajiboye and M. Adeyemi, Upper Bound Analysis for Extrusion at Various Die Land Lengths and Shaped Profiles, *Int. J. Mech. Sci.*, 2007, **49**(3), p 335–351
14. K. Abrinia and H. Davarzani, A Universal Formulation for the Extrusion of Sections with no Axis of Symmetry, *J. Mater. Process. Technol.*, 2012, **212**(6), p 1355–1366
15. K. Abrinia and M. Ghorbani, Theoretical and Experimental Analyses for the Forward Extrusion of Nonsymmetric Sections, *Mater. Manuf. Process.*, 2012, **27**(4), p 420–429
16. T. Altınbalık and A. Onder, Effect of Die Inlet Geometry on Extrusion of Clover Sections Through Curved Dies: Upper Bound Analysis and Experimental Verification, *Trans. Nonferrous Met. Soc. China*, 2013, **23**(4), p 1098–1107
17. P. Karami, K. Abrinia, and B. Saghafi, A New Analytical Definition of the Dead Material Zone for Forward Extrusion of Shaped Sections, *Meccanica*, 2014, **49**(2), p 295–304
18. C. Venkatesh and R. Venkatesan, Design and Analysis of Streamlined Extrusion Die for Round to Hexagon Using Area Mapping Technique, Upper Bound Technique and Finite Element Method, *J. Mech. Sci. Technol.*, 2014, **28**(5), p 1867–1874
19. S.N. Onlaghi and A. Assempour, On the Minimization of the Exit Profile Curvature in Extrusion Through Multi-Hole Dies: A Methodology and Some Verifications, *Meccanica*, 2015, **50**(5), p 1249–1261
20. H. Farzad and R. Ebrahimi, Die Profile Optimization of Rectangular Cross Section Extrusion in Plane Strain Condition Using Upper Bound Analysis Method and Simulated Annealing Algorithm, *J. Manuf. Sci. E Trans. ASME*, 2017, **139**(2), p 021006
21. A.W. Hussein and A.J. Kadhim, Mathematical Analyses and Numerical Simulations for Forward Extrusion of Circular, Square, and Rhomboidal Sections from Round Billets Through Streamlined Dies, *J. Manuf. Sci. E Trans. ASME*, 2017, **139**(6), p 064501
22. H. Haghghat and A. Parghazeh, An Investigation into the Effect of Strain Hardening on the Central Bursting Defects in Rod Extrusion Process, *Int. J. Adv. Manuf. Technol.*, 2017, **93**(1–4), p 1127–1137
23. P. Karami and K. Abrinia, Development of a More Realistic Upper Bound Solution for the Three-Dimensional Problems in the Forward Extrusion Process, *Int. J. Mech. Sci.*, 2013, **74**, p 112–119
24. P. Karami and K. Abrinia, An Analytical Formulation as an Alternative to FEM Software Giving Strain and Stress Distributions for the Three-Dimensional Solution of Extrusion Problems, *Int. J. Adv. Manuf. Technol.*, 2014, **71**(1), p 653–665
25. C. Boer and W. Webster, Direct Upper-Bound Solution and Finite Element Approach to Round-to-Square Drawing, *J. Eng. Ind.*, 1985, **107**(3), p 254–260
26. A.K. Meybodi, A. Assempour, and S. Farahani, A General Methodology for Bearing Design in Non-symmetric T-Shaped Sections in Extrusion Process, *J. Mater. Process. Technol.*, 2012, **212**(1), p 249–261
27. W. Zhou, J. Lin, T.A. Dean, and L. Wang, Feasibility Studies of a Novel Extrusion Process for Curved Profiles: Experimentation and Modelling, *Int. J. Mach. Tool Manuf.*, 2018, **126**, p 27–43
28. Y. Mahmoodkhani, M.A. Wells, N. Parson, and W. Poole, Numerical Modelling of the Material Flow During Extrusion of Aluminium

Alloys and Transverse Weld Formation, *J. Mater. Process. Technol.*, 2014, **214**(3), p 688–700

29. N. Chitkara, K. Abrinia, A Generalised Upper Bound Solution for Three-Dimensional Extrusion of Shaped Sections Using Cad-Cam Bilinear Surface Dies, in *Proceedings of the Twenty-Eighth International* (Springer, 1990), pp. 417–424
30. P. Farahmand, K. Abrinia, A Theoretical Model for the Velocity Field of the Extrusion of Shaped Sections Taking into Account the Variation

of the Axial Component, in *Proceedings of the 36th International MATADOR Conference*, (Springer, 2010), pp. 53–57

Publisher's Note Springer Nature remains neutral with regard to jurisdictional claims in published maps and institutional affiliations.